J|A|C|S
ARTICLES

Detecting Vascular Biosignatures with a Colloidal, Radio-Opaque Polymeric Nanoparticle

Dipanjan Pan,* Todd A. Williams, Angana Senpan, John S. Allen, Mike J. Scott, Patrick J. Gaffney,[†] Samuel A. Wickline, and Gregory M. Lanza

C-TRAIN and Division of Cardiology, Washington University School of Medicine, 4320 Forest Park Avenue, Saint Louis, Missouri 63108 and Department of Surgery, St Thomas's Hospital, London, U.K.

Received August 11, 2009; E-mail: dipanjan@wustl.edu

Abstract: A synthetic methodology for developing a polymeric nanoparticle for targeted computed tomographic (CT) imaging is revealed in this manuscript. The work describes a new class of soft type, vascularly constrained, stable colloidal radio-opaque metal-entrapped polymeric nanoparticle using organically soluble radio-opaque elements encapsulated by synthetic amphiphile. This agent offers several-fold CT signal enhancement in vitro and in vivo demonstrating detection sensitivity reaching to the low nanomolar particulate concentration range.

Introduction

In spite of innumerable medical advances in the detection of severe carotid and coronary artery stenosis, sensitive detection, and differentiation of vulnerable versus stable atherosclerotic plaques in vessels with mild severity stenosis remains restricted with angiography, irrespective of modality.[1] Others and we have demonstrated the use of magnetic resonance (MR) molecular imaging for the detection of microthrombi in ruptured plaques.[2] However, the feasibility of this approach is strikingly limited by the motion of the heart in the coronary tree.[3] Multislice CT (MDCT) has emerged as a promising modality for noninvasive coronary angiography (CA). At present, 64 slice scanners can produce contrast-enhanced angiograms in less than 25 ms and the ultimate advancement of up to 256 slice scanners will allow entire acquisitions within one heart cycle.[4] The evolution of CT in the clinic now includes dual-energy CT, which, by various vendor-dependent means, improves the differentiation of bio-

logical tissues including bone from contrast materials, such as iodine or heavier metal-based agents.[4] Already in development and poised for commercial translation in the next decade are high-resolution multichannel CT systems, sometimes referred to as Spectral CT. These, instruments utilize unique detectors designed to recognize and quantify the K-edge energy signature of metals within the X-ray bandwidth (e.g., gold, gadolinium, or bismuth) with higher spatial and energy resolution.

Developing contrast agents with prerequisite features for molecular CT continues to remain a challenge. The insensitivity of X-ray-based imaging techniques mandates the development of nanoparticles with very high radio-opaque material densities while maintaining particle integrity on the shelf and in circulation. The core radio-opaque materials must be resistant to biometabolism and completely bioeliminated after systemic use. A number of nanoparticulate contrast agents based on metallic nanocrystals (hard-particle approach) for CT have been suggested recently,[5,6] but only a few were shown to have the potential for targeted imaging.[6] Moreover, particles based on heavy-metal crystals are poorly metabolized and the crystals size (>10 nm) may preclude elimination through the urine or bile, presenting a regulatory challenge to prove long-term safety.

Our development of vascular-targeted molecular CT agents, a major and mostly uninvestigated task, has been directed toward

* To whom correspondence should be addressed.
† Washington University School of Medicine.

(1) (a) Zoler, M. L. *Cardiology News* **2007**, *5* (12), 1. (b) Brown, B.; Gallery, C.; Badger, R. *Circulation* **1986**, *73*, 653–661.
(2) (a) Winter, P. M.; Caruthers, S. D.; Wickline, S. A.; Lanza, G. M. *Nanofabrication Towards Biomedical Applications* **2005**, 227–49. (b) Pan, D.; Wickline, S. A.; Lanza, G. M.; Caruthers, S. D. *Eur. J. Radiol* **2009**, *70* (2), 274. (c) Botnar, R. M.; Perez, A. S.; Witte, S.; Wiethoff, A. J.; Laredo, J.; Hamilton, J.; Quist, W.; Parsons, E. C.; Vaidya, A.; Kolodziej, A.; Barrett, J. A.; Graham, P. B.; Weisskoff, R. M.; Manning, W. J.; Johnstone, M. T. *Circulation* **2004**, *109*, 2023. (d) Nair, S. A.; Kolodziej, A. F.; Bhole, G.; Greenfield, M. T.; McMurry, T. J.; Caravan, P. *Angew. Chem., Int. Ed.* **2008**, *47*, 4918. (e) Hu, G.; Lijowski, M.; Zhang, H.; Partlow, K. C.; Caruthers, S. D.; Kiefer, G.; Gulyas, G.; Athey, P.; Scott, M. J.; Wickline, S. A.; Lanza, G. M. *Int J Cancer.* **2007**, *120* (9), 1951–7. (f) Winter, P. M.; Schmieder, A. H.; Caruthers, S. D.; Keene, J. L.; Zhang, H.; Wickline, S. A.; Lanza, G. M. *FASEB J.* **2008**, *22* (8), 2758–67. (g) Schmieder, A. H.; Winter, P. M.; Caruthers, S. D.; Harris, T. D.; Williams, T. A.; Allen, J. S.; Lacy, E. K.; Zhang, H.; Scott, M. J.; Hu, G.; Robertson, J. D.; Wickline, S. A.; Lanza, G. M. *Magn. Reson. Med.* **2005**, *53* (3), 621–7.
(3) Hofman, M. B. M.; Wickline, S. A.; Lorenz, C. H. *J. Mag. Res. Imag.* **1998**, *8* (3), 568–576.
(4) (a) Horiguchi, J.; Fujioka, C. *AJR Am. J. Roentgenol.* **2007**, *189* (4), 981–8. (b) Thieme, S. F.; Johnson, T. R.; Lee, C.; McWilliams, J.; Becker, C. R.; Reiser, M. F.; Nikolaou, K. *AJR Am. J. Roentgenol.* **2009**, *193* (1), 144–9. (c) Schlomka, J. P.; Roessl, E.; Dorscheid, R.; Dill, S.; Martens, G.; Istel, T.; Bäumer, C.; Herrmann, C.; Steadman, R.; Zeitler, G.; Livne, A.; Proksa, R. *Phys. Med. Biol.* **2008**, *53* (15), 4031–4047.
(5) (a) Rabin, O.; Manuel, P. J.; Grimm, J.; Wojtkiewicz, G.; Weissleder, R. *Nat. Mater.* **2006**, *5* (2), 118–22. (b) Ashcroft, J.; Gu, M.; Zhang, W. T.; Hughes, M. S.; Hartman, K. B.; Hofmann, C.; Kanaras, A. G.; Kilcoyne, D. A.; Le Gros, M.; Yin, Y.; Alivisatos, A. P.; Larabell, C. A. *Chem. Commun.* **2008**, *7* (21), 2471–2473.
(6) (a) Hainfeld, J. F.; Slatkin, D. N.; Focella, T. M.; Smilowitz, H. *Br. J. Radiol.* **2006**, *79*, 248–253. (b) Hainfeld, J. F.; Slatkin, D. N.; Smilowitz, H. M. *Phys. Med. Biol.* **2004**, *49*, N309–N315.

the design of nanometric colloids without utilization of metal crystals, that is, so-called soft particles. Whereas other polymeric and dendritic nanoparticle-based platforms of soft (approximately 50 nm or less) nature have been studied previously for molecular imaging application,[7] soft particles less than 50 nm typically distribute extravascularly throughout tissues and introduce confounding nonspecific signal from off-target binding to cells or tissues presenting similar biomarkers and from entrapment of particles with the interstital milieu.

Toward this aim, we present a novel approach based on a soft colloidal, radio-opaque, and metal-encapsulated polymeric (*c*ROMP) nanoparticle with ~30 wt % metal content using noncrystalline organically soluble radio-opaque elements encapsulated by amphiphilic diblock copolymers, which can be homed specifically to vascular targets. The design of the *c*ROMP nanoparticles is based on the self-assembly of amphiphilic diblock copolymer in aqueous media to entrap high payloads of radio-opaque elements (in millions). The particles are cross-linked on the surface to enhance shelf life stability and particle integrity in vivo. The availability of the surface functional groups facilitates the presentation of homing agents for high avidity cell-specific targeting. The particles incorporate millions of organically soluble radio-opaque small molecules, which are anticipated to clear from the body through the kidney or biliary system.

Results and Discussion

We report a synthetic methodology for developing a polymeric molecular imaging agent designed for use with computed tomography (CT). The work describes a unique soft colloidal nanoparticle in which very high concentrations of radio-opaque elements are in a form of organometallics or organically soluble complexes incorporated into the core to establish adequate CT contrast when bound to a biological target. To prevent the small organometallic molecules (and complexes) used in the *c*ROMP particle from rapidly extravasating into tissues or clearing through the kidney, they have been encapsulated within a larger, vascular-constrained (~150 nm) colloidal particle, which can improve targeting specificity for intraluminal thrombus. In a typical synthesis, PS-*b*-PAA[8] (Mn × 10^{-3}: 0.8-*b*-29.3 polydispersity index: PDI = 1.18, 0.0033 mmol) was dissolved in a mixture of methanol and chloroform (4:1) and subjected to controlled evaporation under reduced pressure to generate a thin film of polymer. The thin film was dispersed in deionized water (0.2 μM) by probe sonication at ambient temperature. Ethiodized oil (ethiodol: a mixture of iodostearic acid ethyl ester and
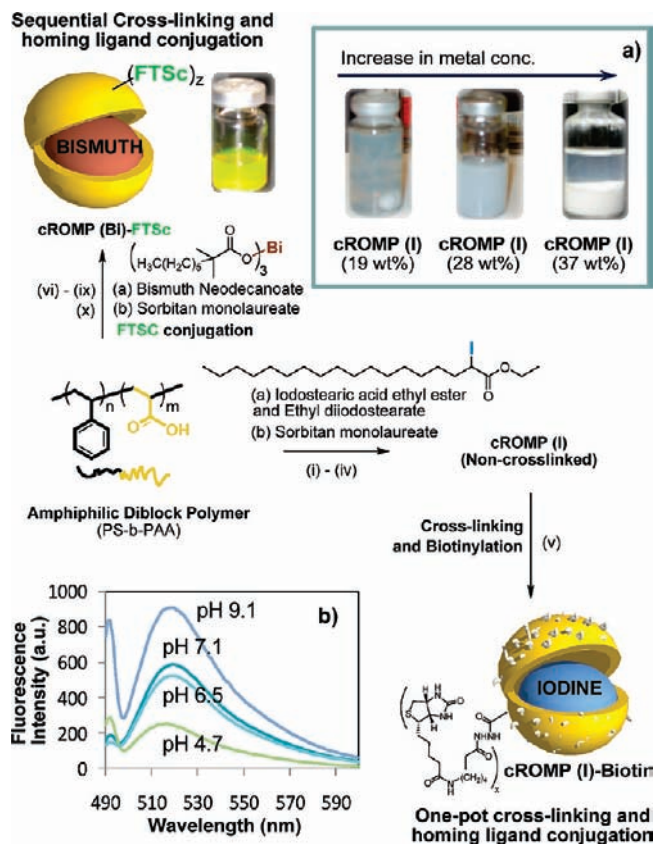

Figure 1. Preparation of *c*ROMP nanoparticles: (i) Suspension of Ethiodol in polysorbate, vortex, and mixing; (ii) thin-film formation from PS-*b*-PAA;[8] (iii) dispersion of the thin film in water (0.2 μM); (iv) microfluidization at 4 °C, 137.9 MPa, dialysis (v) 2,2′-(ethylenedioxy) bis(ethylamine), EDCI, and biotin hydrazide, dialysis (cellulosic membrane, MWCO 20 K); (vi) suspension of bismuth neodecanoate in polysorbate, vortex, and mixing; (vii) thin-film formation from PS-*b*-PAA; (viii) dispersion of the thin film in water (0.2 μM); (ix) microfluidization at 4 °C, 137.9 MPa, dialysis (cellulosic membrane, MWCO 20K); 2,2′-(ethylenedioxy) bis(ethylamine), EDCI; dialysis; (x) fluorescein thiasemicarbazide (FTSC), EDCI, dialysis; (a) optical pictures of replicates of *c*ROMP(I); (b) pH sensitive fluorescence from FTSC labeled *c*ROMP(Bi) (λ_{ex} = 496 nm; λ_{em} = 510 nm).

ethyldiiodostearate;[9] 37 wt % of total iodine content) was suspended in polysorbate (sorbitan monolaurate (5 vol %) and microfluidized with PS-*b*-PAA dispersion (0.5 vol %) to obtain the *c*ROMP (iodine) particle. The design of the *c*ROMP nanoparticles minimized the use of the PS block segment (only 3% contribution from the hydrophobic segment), which has been associated with biocompatibility issues.[8e] The particle thus formed was immediately subjected to a carbodiimide-mediated intramolecular cross-linking (Figure 1) in the presence of diamine linker followed by the one-pot reaction of amine-terminated homing agent with the remaining PAA carboxyl groups. The cross-linking improved the shelf-life stability of the nanoparticles and further ensured the structural integrity of the nanoparticles in vivo.

The cross-linking[10] was accomplished by condensation reactions of 2,2′-(ethylenedioxy) bis(ethylamine) with the acrylic acid residues along the PAA segments (0.5 equiv amine-to-acid functionalities), facilitated by 1-(3′-dimethylaminopropyl)-

(7) (a) Majoros, I. J.; Baker, J. R., Jr. *Dendrimer Based Nanomedicine*, Edited Book, Pan Stanford Pb. 2008. Hawker, C. J.; Wooley, K. L. *Science* **2005**, *309*, 1200–5. (c) O'Reilly, R. K.; Hawker, C. J.; Wooley, K. L. *Chem. Soc. Rev.* **2006**, *35*, 1068–83. (d) Fu, Y.; Nitecki, D. E.; Maltby, D.; Simon, G. H.; Hans-Juergen, K. B.; Yeh, R. B. M.; Shames, D. M.; Brasch, R. C. *Bioconjugate Chem.* **2006**, *17* (4), 1043–1056.

(8) (a) Laruelle, G.; François, J.; Billon, L. *Macromol. Rapid Commun.* **2004**, *25* (21), 1839–1844. (b) Huang, H.; Kowalewski, T.; Remsen, E. E.; Gertzmann, R.; Wooley, K. L. *J. Am. Chem. Soc.* **1997**, *119* (48), 11653–11659. (c) Wu, J.; Eisenberg, A. *J. Am. Chem. Soc.* **2006**, *128* (9), 2880–2884. (d) Xu, J.; Sun, G.; Rossin, R.; Hagooly, A.; Li, Z.; Fukukawa, K. I.; Messmore, B. W.; Moore, D. A.; Welch, M. J.; Hawker, C. J.; Wooley, K. L. *Macromolecules* **2007**, *40* (9), 2971–2973. (e) Avital, A.; Shapiro, E.; Doviner, V.; Sherman, Y.; Margel, S.; Tsuberi, M.; Springer, C. *Am. J. Respir. Cell Mol. Biol.* **2002**, *27* (4), 511–4.

(9) Stanbury, J. B.; Barnaby, J.; Daza, G. 2002. Recommendations for the use of iodized oil, http://icb.usp.br/lats/STAMBURY.HTM, accessed on September 17.

(10) Pan, D.; Turner, J. L.; Wooley, K. L. *Chem. Commun.* **2003**, 2400–2401.
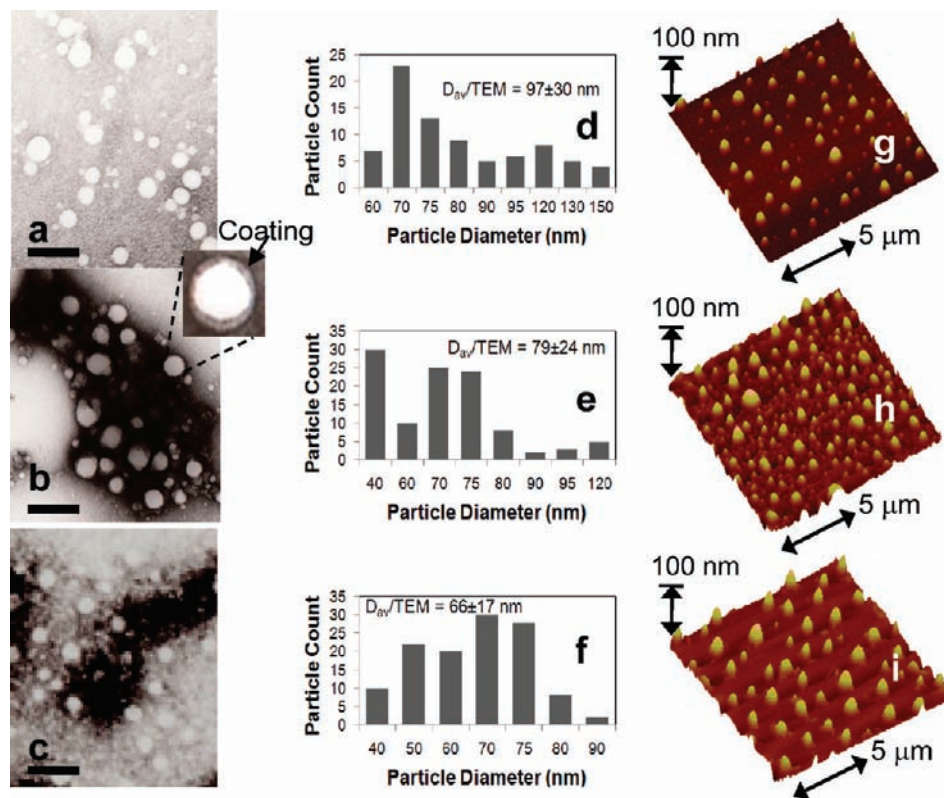
Figure 2. Characterization of cROMP: (top) dried state TEM images of (a,b) cROMP(Iodine), 28 wt % and 19 wt %, (c) cROMP(Bismuth) (uranyl acetate; scale bar = 300 nm); (d−f) particle size distributions of cROMP(I) (19 wt %), cROMP(I) (28 wt %), and cROMP(Bi); dried state AFM images of (g−h) cROMP (iodine), 28 wt % and 19 wt %, respectively, (i) cROMP (Bismuth); (bottom) physico-chemical characterization table.

3-ethylcarbodiimide methiodide (1.2 equiv based upon acrylic acid groups). Conjugation of the homing agent (e.g., biotin) onto the cross-linked cROMP particle was performed within the same reaction vessel, with the introduction of biotin hydrazide by allowing it to undergo amidation-based attachment to preformed cross-linked cROMPs bearing carboxylic acids within their surface. The nanoparticle was purified by exhaustive dialysis against infinite sink of nanopure water using cellulosic dialysis membrane (20 kDa MWCO). This synthesis resulted in an encapsulation of 2 304 841 iodine atoms (ICP-MS = 12 mg of iodine /ml) and nominally 1000 biotins per nanoparticle for biotin−avidin interaction. The entrapment efficiency was calculated to be ∼96%. A control nanoparticle was prepared identically except for the inclusion of the ethiodol. The iodinated-cROMP (I) particles, thus formed, had nominal hydrodynamic diameter of 162 ± 3 nm as measured by dynamic light scattering (DLS). The polydispersity and zeta potential were measured as 0.26 ± 0.01 and -20 ± 6 mV (Brookhaven Instrument Co.), respectively. The dehydrated state diameter (D_{av}) and height parameters (H_{av}) of the cROMP (I) were 97 ± 30 and 78 ± 24 nm, as measured by transmission electron microscopy (TEM) and atomic force microscopy measurements (AFM) respectively (Figure 2). The discrepancies in hydrodynamic diameter (DLS) and height values (AFM) reflected partial flattening of the soft nanoparticles on the glass substrates which is characteristics of these polymers as reported earlier.[8d]

The presence of polysorbate as an amphiphatic core matrix was found to be critical in the formulation of cROMP, as apparent from the reduced entrapment efficiency of metal, premixed with a lower concentration of sorbitan monolaureate. Our preliminary effort to formulate a particle with exclusively ethiodol core (100% v/v) was unsuccessful. Particles with poor
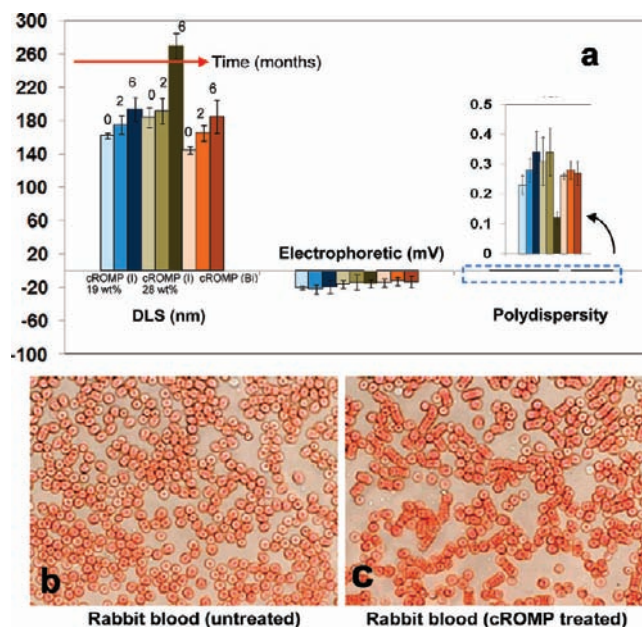

Figure 3. (a) Stability of iodinated and bismuth-encapsulated cROMP: Measurements of hydrodynamic diameter (DLS), electrophoretic potential (zeta), and polydispersities (PDI) over 6 months; optical microscopy images of blood smear untreated (b) and treated with cROMP (c) (magnification: 40×).

shelf life stability were produced with a ratio 9:1 (v/v) of ethiodol and polysorbate concentration (optical pictures Figure 1a). Stability of these particles were further investigated by monitoring the changes in the particle size and zeta potential of these colloids over six months. As evident from Figure 3,
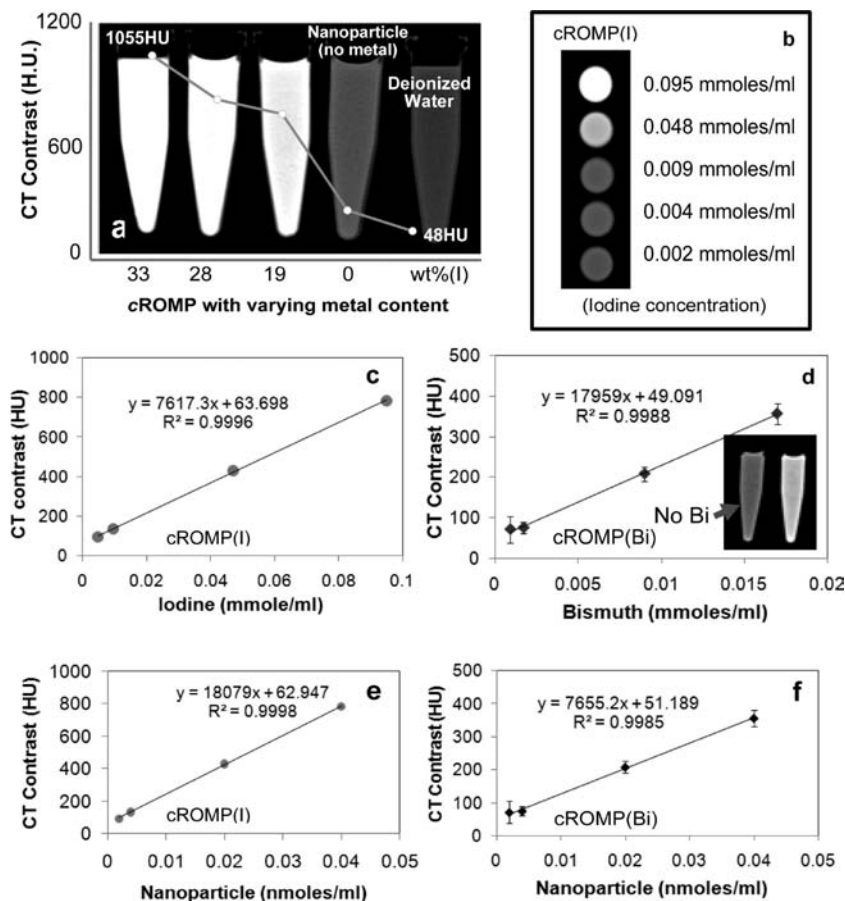
Figure 4. CT imaging in suspension: (a) CT opacity as a function of concentration generated from centrifuge tubes (internal diameter, i.d. 10 mm; outer diameter, o.d. 13 mm; vol, 1 cc) filled with *c*ROMP (iodine) with varying concentration of metal, control nanoparticle (no metal) and water; (b) cross sectional CT images of serially diluted *c*ROMP nanoparticles; variation of CT signal (HU) with metal (c: iodine, 19 wt %; d: bismuth, 7 wt %) and nanoparticles (particulate) concentration (e,f).
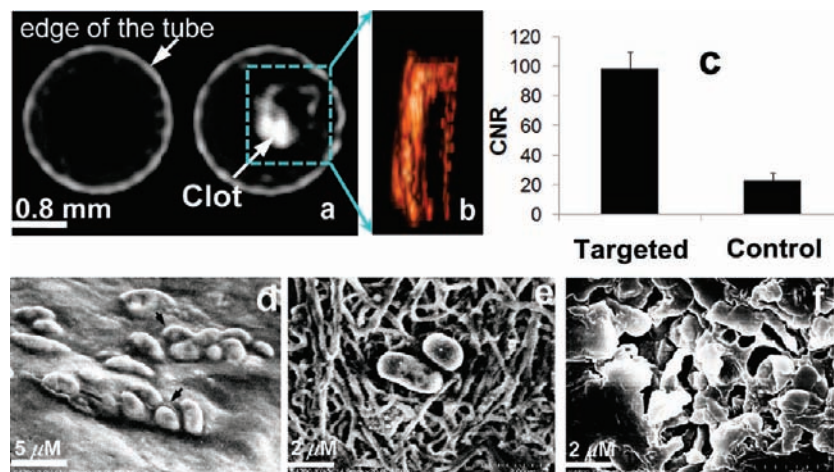

Figure 5. In vitro targeting: (a) representative CT images of human plasma clots treated with *c*ROMP (left, nontargeted control, no biotin) and *c*ROMP (right, targeted, with biotin); the clots treated with control *c*ROMP particles are impossible to distinguish from the surrounding water; (b) the volume rendered view of the targeted clot; (c) contrast-to-noise ratio from targeted and control clots; SEM images of the clots show target specific localization of biotinylated-*c*ROMP nanoparticles: (d) partially dried clots, (e) dried clot exhibits the fibrin strands (f) dried clot after gold coating (grain size of the gold, 5−10 Å; coating thickness, ∼25−50 Å).

the particle size (hydrated state), electrophoretic potential (zeta), and polydispersities have varied less than 5% when stored at 4 °C under argon in sealed serum vials. A blood smear preparation[11] was performed to observe morphological changes in lymphocytes and blood clumping using clinical microscopy technique (conventional light microscopy) under high-power field. No significant clumping or morphological changes in blood cells were observed in animals treated with *c*ROMP (blood: NP = 9:1) (experimental details in the Supporting Information).

The present methodology could be extended to feature other metals, for example, bismuth, gold, titanium, and so forth. To test this hypothesis, an identical procedure was followed that
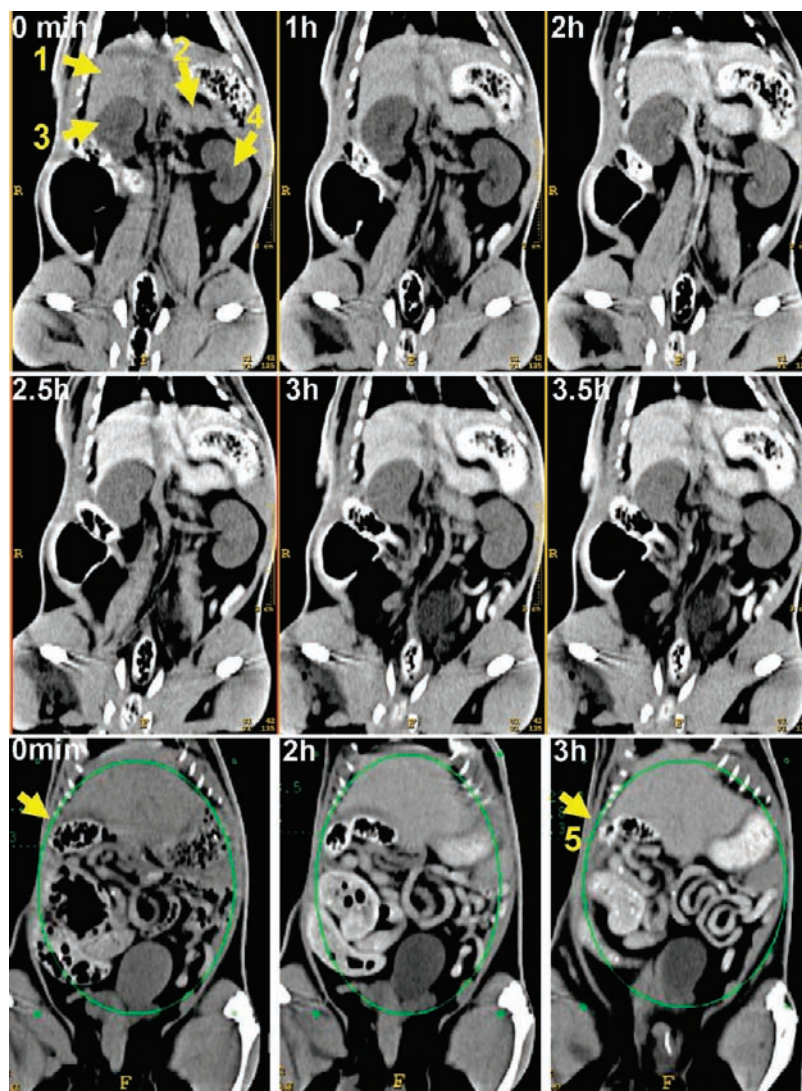
Figure 6. In vivo CT imaging: (top) coronal reconstructed serial CT images of a rat following tail-vein injection of *c*ROMP (6 mL/kg) showing the clear delineation of the major organs i.e. liver (1), spleen (2), kidney (3, 4), and gastrointestinal track (5).

utilized bismuth neodecanoate (Aldrich, Inc.) to synthesize noncross-linked *c*ROMP (Bi) incorporating 3530 μg/g bismuth (ICP-MS) (Figure 1). The nanoparticles thus formed were immediately subjected to a sequential carbodiimide-mediated intramolecular cross-linking and attachment of biologically relevant agents (e.g., fluorescein thiosemicarbazide, FTSC) (Figure 1). Approximately 396 649 bismuth atoms (ICP-MS= 3.5 mg of Bi/ml, entrapment efficiency = 78%) were encapsulated by this protocol as determined by ICP-MS. This resulted in nanoparticles with hydrodynamic diameter of 145 $\pm$ 10 nm (DLS), zeta potential (-14 ± 5 mV), D_{ah} (66 $\pm$ 17 nm), and H_{av} (71 $\pm$ 36 nm), respectively (Figure 2). This confirms the presence and chemical availability of the carboxylic acid groups throughout the nanoparticle shell. FTSC conjugated nanoparticles also exhibited pH sensitive fluorescence spectra within pH ranges of 4.7−9.1 (part b of Figure 1). The ability of the fluorescent-labeled *c*ROMP nanoparticles to change their color within this physiological range may provide increased sensitivity required for optical pH measurements inside the live cell.

Several CT imaging experiments were performed next with iodinated and bismuth-*c*ROMP particles in suspension. Part a of Figure 4 shows the CT images of *c*ROMP (I) particles, nonmetallic nanoparticles, and water in a centrifuge tube (0.95 mL). The overlapping plot indicates experimental CT opacities of 33 wt % (1055 $\pm$ 120 HU), 28 wt % (904 $\pm$ 82 HU), 19 wt % (720 $\pm$ 25 HU), nonmetalated nanoparticles (48 $\pm$ 7), and water ((48 $\pm$ 6). Part b of Figure 4 shows the cross-sectional CT images of the centrifuge tubes filled with serially diluted *c*ROMP replicates. The attenuation of *c*ROMP formulations varied linearly as a function of metal concentration (iodine, r^2 = 0.999 for 19 wt %; and bismuth, r^2 = 0.998) (parts c and d of Figure 4) and nanoparticle concentration (iodine, r^2 = 0.999; and bismuth, r^2 = 0.998) (parts e and f of Figure 4). The higher CT coefficient (part d of Figure 4) of *c*ROMP (Bi) based on metal concentration can be attributed to the high atomic number of Bi (Z = 83) in comparison with iodine (Z = 53, part c of Figure 4). However, the high CT coefficient value of the iodinated formulation reflected a 19 wt % particle metal content versus 7 wt % for the bismuth agent used in this comparison (parts e and f of Figure 4). Further-optimized bismuth *c*ROMP is expected to approach 28 wt % or more, similar to the iodine example.

Whereas these molecular CT imaging agents would potentially have broad applicability for many disease types, for this

(11) Wheater, P. R.; Burkitt, H. G.; Daniels, V. G. *Functional Histology*, Longman Group: U.K.; page 407.

in vitro research fibrin, a vital element of intravascular thromboses, was the focus. Biotinylated *c*ROMP (I) (19 wt %) and a control *c*ROMP nanoparticle (no biotin) were targeted to acellular fibrin clot phantoms with classic avidin−biotin interactions using a well-characterized biotinylated antihuman fibrin-specific monoclonal antibody (NIB5F3).[12] Axial CT images of the centrifuge tubes (sealed polystyrene test tubes; vol., 3 cc, 75 mm) are shown in Figure 5 containing targeted fibrin clots on suture, suspended in deionized water. Cross-sectional CT images of the plasma clot (treated with control *c*ROMP) and plasma clot targeted with biotinylated *c*ROMP (with iodine) respectively were acquired using a Philips Precedence (Brilliance) 16 channel CT imaging system. The control clot produced negligible contrast (19 ± 3 HU) and could not be differentiated from the surrounding medium (water) (part a of Figure 5 (left)). The targeted fibrin clot on the other hand revealed much higher attenuation (136 ± 11 HU) in the CT image (part a of Figure 5 (right)) allowing them to be distinguished from the surrounding water (CNR = 98 ± 12). The volume-rendered CT image (part b of Figure 5) of the targeted clot revealed the fine configuration of irregularly shaped clot targeted with *c*ROMP.

High-resolution scanning electron microscopic (SEM) analyses of the targeted fibrin clots support the successful target specific localization of biotinylated-*c*ROMP nanoparticles. The partially dried clot (targeted) showed that the particles were aggregated on the clots (part d of Figure 5). Once the clot was dried for 24−48 h (class 1000 clean room), the fibrin stands became more prominent (part e of Figure 5) and revealed the particles attached to the surface of the clot. The compliant nanoparticles were found to flatten out considerably with drying. Further, after coating with gold (part f of Figure 5), it appeared that the gold partially filled areas around the fibrin and the targeted particles. The grain size of the gold was on the order of 5−10 Å with a coating thickness of ∼25−50 Å.

In vivo CT blood-pool imaging was performed in a rat model ($n = 2$) to provide a preliminary assessment of in vivo contrast, pharmacokinetics, and biodistribution using an intravenous dose of 6 mL/kg, 0.28 mmole of iodine/kg, which is 6-fold greater than typically employed for molecular imaging applications.[2e−g] In molecular imaging studies, low circulating concentrations of metal are required for negligible background contrast; the detectability of target signal evolves with time as the homed metal-rich particles bind and accumulate. Following intravenous administration of *c*ROMP into rat, serial CT imaging was performed to determine the blood half-life and organ distribution. The CT enhancement of left cardiac ventricle and intra vena cava was monitored over a period of 3.5 h. The blood half-life in rat was 56 ± 6 min (biexponential decay), which is six times longer than commercially available iodine contrast agents (<10 min) to obtain blood pool coronary angiograms, adequate for ligand-targeted saturation of fibrin epitopes, and rapid enough to eliminate background blood signal and permit molecular imaging targeted thrombus within 2 h post contrast injection. The significant enhancement of CT signal (CNR = ∼48) of the anterior abdominal cavity including the liver, gastrointestinal track, and stomach (area = 3 500 mm²) was observed at its peak. The enhancement resulted in improved delineation of the major organs, which suggested that the *c*ROMP had distributed into major reticuloendothelial clearance organs, typical of nanoparticulate molecular imaging agents.[2e−g] These data further suggest that the organometal complexes were being bioeliminated primarily through biliary routes as suggested by the 50-fold increase in contrast noted in the gastrointestinal tract (Figure 6). However, more in-depth study is required to establish these response parameters.

Conclusions

In summary, we have successfully demonstrated the feasibility of molecular CT with a novel polymeric nanoparticulate agent. *c*ROMP nanoparticles offer several-fold CT signal enhancement in suspension and in vitro demonstrating detection sensitivity reaching to the low nanomolar particulate concentration range. The in vitro images of the human plasma clots targeted with biotinylated nanoparticle and in vivo imaging in rats further exemplify the feasibility of intravascular CT with *c*ROMP nanoparticle. Although more in-depth animal studies will be necessary to understand the behavior of each component in vivo, the synthesis of *c*ROMP nanoparticles employed general pharmaceutically accepted components such as polysorbates, glycerin, and so forth, which should facilitate its clinical translation.

Supporting Information Available: Experimental details and characterization data. This material is available free of charge via the Internet at http://pubs.acs.org.

JA906797Z

(12) Raut, S.; Gaffney, P. J. *Thromb. Haemostasis* **1996**, *76*, 56.